Journal of Sound and Vibration (2001) **240**(5), 821–836
doi:10.1006/jsvi.2000.3288, available online at http://www.idealibrary.com on IDEAL®

RESONANT-OVERLAP PHENOMENA IN STOCHASTIC LAYERS OF NON-LINEAR HAMILTONIAN SYSTEMS WITH PERIODICAL EXCITATIONS

A. C. J. Luo

*Department of Mechanical and Industrial Engineering, Southern Illinois University Edwardsville, Edwardsville, IL*62026-1805, *U.S.A. E-mail: aluo@siue.edu*

(*Received* 9 *April* 1999, *and in final form* 20 *July* 2000)

An accurate standard-map approach, instead of the approximate standard-map approach, is developed for the analytical prediction of the onset of a new resonant overlap forming a new resonant-separatrix web in the stochastic layer. This accurate approach applies to the twin-well Duffing oscillator for illustration of the resonant overlap phenomena in stochastic layers. The excitation strengths are obtained analytically for the onset of the specified resonant-separatrix webs in the stochastic layer. This accurate approach gives a very good prediction compared to numerical results for the lower order resonant overlap. When excitation strength is very weak, the accurate and approximate standard-map methods are in good agreement, and the accurate one is applicable to non-linear systems with strong excitations. However, the further improvement should be completed for a more accurate, analytical prediction of the onset of a new resonant overlap in stochastic layers of non-linear Hamiltonian systems with periodical excitations.

1. INTRODUCTION

The chaotic motion in a non-linear Hamiltonian system is formed through resonant interactions. These interactions result in resonant overlap phenomena, and such a chaotic motion is also characterized by the resonance. In 1964, Henon and Heiles [1] first observed internal resonant layers of a two-degrees-of-freedom (d.o.f.) non-linear system numerically. Stochasticity in a motion layer in the neighborhood of the resonant separatix is generated by the deterministic Hamilton's equations without additional *ad hoc* "stochastic" forces. When the stochasticity goes from being local to global, the motion in the motion layer becomes chaotic, and the motion layer is termed the resonant layer. Therefore, the resonant layer is a domain of chaotic motion in the vicinity of the resonant separatrix. A similar definition is given in Lichtenberg and Lieberman [2, p. 51]. In 1998, Han and Luo [3] developed an accurate standard-map approach for the prediction of the onset of resonant layers in non-linear dynamical systems. In 1999, Luo and Han [4] also used a modified Chirikov overlap criterion to predict of the resonant layer appearance. In the same year, Luo *et al.* [5] developed an energy spectrum method for numerical predictions of the onset of resonance in the stochastic layer. In this paper, such a standard-map approach will be presented for the investigation of the resonant overlap characteristics in the stochastic layers of non-linear systems. The stochastic layer first described in reference [6] is the domain of chaotic motion in the vicinity of the separatrix. For explanation of such a chaotic motion in non-linear Hamiltonian systems, consider a Hamiltonian system possessing a homoclinic orbit (or separatrix). When an external, periodic forcing acts on the

0022-460X/01/100821 + 16 $35.00/0

Hamiltonian system, many resonances appear in the neighborhood of the separatrix, as illustrated in Figure 1 though the twin-well Duffing oscillator. The resonant conditions are obtained from the energy analysis of the non-linear system. Each resonance has its own separatrix, and the characteristics of the resonant separatrix to its sub-resonance are similar to the non-resonant separatrix. When chaos occurs, the self-similarity can be developed through renormalization group technique (see reference [2]).

The earlier, quantitative studies of the stochastic layers were presented in references [6, 7] even though the chaotic motion in the neighborhood of the separatrix was qualitatively described [8] in 1899. In 1968, Zaslavsky and Filonenko [6] first introduced the approximate separatrix map (or whisker map [9]) to investigate the one-dimensional motion of a charged particle in the field of a travelling wave under a perturbation. The approximate separatrix map is derived under the following three assumptions. (1) The first complete elliptic integral is approximated by $K(k) \approx \log(4/\sqrt{1-k^2})$ when periodic orbits of the unperturbed system are close to the separatrix (e.g., reference [10]). (2) Only the period of the libration is used for the estimate of phase change, without the rotation. (3) The energy change is computed through the separatrix [9, 11]. For the stochastic instability of trapped particles, Zaslavsky and Filonenko [6] also linearized the whisker map into a standard map in the neighborhood of an assumed resonance. Therefore, the following two additional assumptions are adopted. (4) The whisker map is approximated at the period-1 fixed point based on a primary resonance. (5) The primary resonant condition is assumed but not derived from the original dynamic systems. A similar procedure was used to investigate the chaotic motion in the vicinity of the separatrix under high-frequency excitation [12]. From the energy analysis of non-linear systems, the resonant motions in regions separated by the separatrix in phase space distinguish themselves [4, 13, 14]. Therefore, such a standard-map approach cannot provide a satisfactory prediction of the stochastic layer for the original system.

In recent years, the approximate whisker map is used extensively because it provides a better prediction of the stochastic layer than the standard map [15–22]. For the energy

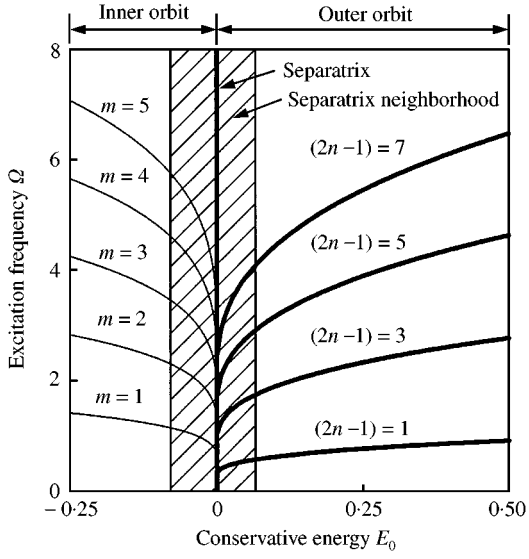

Figure 1. Resonant conditions in the neighborhood of separatrix for the twin-well-Duffing oscillator ($\alpha_1 = \alpha_2 = 1{\cdot}0$).

increment computation, in 1995, Zaslavsky and Abdullaev [16] introduced a shifted separatrix map. In 1990, Rom-Kader [20] derived the approximate whisker map through the Melnikov function and used the whisker map to predict transport rates statistically and numerically. The escape rates in the vicinity of homoclinic tangles were investigated [21], but assumptions (1)–(3) were still used to derive the approximate whisker map. In 1995, Rom-Kader [22] determined the secondary homoclinic bifurcation through the simple zero of the Hamiltonian energy at the second iteration of the approximate whisker map. In 1998, Treschev [23] presented a qualitative relationship between the width (w) of the stochastic layer and the width (d) of the lobe domain, such as $w/d \sim 1/\log \mu$ and μ is a multiplier at the corresponding hyperbolic point.

Reichl and Zheng [24, 25] estimated the width of the stochastic layer (actually, excitation strength) for the undamped Duffing oscillator through the approximate standard-map approach and Chirikov overlap criterion presented in reference [10]. The Chirikov overlap criterion usually gives the correct order of magnitude for excitation strength even though the self-similarity of resonance is ignored. To address the self-similarity of resonance, the renormalization group technique was proposed for the estimate of excitation strength in references [26, 27]. In 1986, Lin and Reichl [28] used this technique to investigate the chaotic motion of a particle in an infinite square well potential. For the Chirikov overlap criterion and the renormalization group technique, only two of the infinite primary resonances are modelled.

From the above literature survey, the resonant overlap phenomena in stochastic layers need to be further investigated. In this paper, an accurate standard-map approach is developed for the prediction of the onset of the resonant-separatrix web formed through the resonant overlap. This approach applies to the twin-well-potential-Duffing oscillator for illustrations of the stochastic layer. Based on the approximate standard-map approach, the prediction of excitation strengths for the stochastic layer in the Duffing oscillator is also presented.

2. AN ACCURATE STANDARD-MAP APPROACH

Consider a non-linear Hamiltonian system:

$$\dot{\mathbf{x}} = \mathbf{f}(\mathbf{x}) + \mathbf{g}(\mathbf{x}, t), \quad \mathbf{x} = \begin{pmatrix} x \\ y \end{pmatrix} \in \Re^2, \tag{1}$$

where $\mathbf{f}(\mathbf{x})$ is an unperturbed Hamiltonian vector field on $\Re^2$ and $\mathbf{g}(\mathbf{x}, t)$ is periodic in time with period $T = 2\pi/\Omega$, and

$$\mathbf{f}(\mathbf{x}) = \begin{pmatrix} f_1(\mathbf{x}) \\ f_2(\mathbf{x}) \end{pmatrix} \quad \text{and} \quad \mathbf{g}(\mathbf{x}, t) = \begin{pmatrix} g_1(\mathbf{x}, t) \\ g_2(\mathbf{x}, t) \end{pmatrix} \tag{2}$$

are sufficiently smooth ($C^r, r \geqslant 2$) and bounded on bounded sets $D \subset \Re^2$ in phase space. Consider the system in equation (1) possessing the total Hamiltonian $H(\mathbf{x}, t) = H_0(\mathbf{x}) + H_1(\mathbf{x}, t)$ in which $H_1(\mathbf{x}, t)$ is a perturbation of Hamiltonian, and

$$f_1 = \frac{\partial H_0}{\partial y}, \qquad f_2 = -\frac{\partial H_0}{\partial x}, \qquad g_1 = \frac{\partial H_1}{\partial y}, \qquad g_2 = -\frac{\partial H_1}{\partial x}. \tag{3}$$

Because the stochastic layer is formed in the vicinity of the separatrix [8], the perturbed orbit of equation (1) intersects with at least three families of its unperturbed periodic orbits,

as shown in Figure 2. Such periodic orbits are termed (α, β, γ)-orbits for convenience. Under the periodic perturbation, the stochastic layer of equation (1) in the vicinity of separatrix $(q_0(t))$, illustrated in Figure 3, consists of σ-sub-layers pertaining to the $q_\sigma(t)$-orbits $(\sigma = \alpha, \beta, \gamma)$. For any σ-layer, the changes of energy H_0 and phase φ, for time transition from t_i to $t_i + T_\sigma$ in equation (1), give a discrete map:

$$E_{i+1} = E_i + \Delta H^\sigma(\varphi_i) \quad \text{and} \quad \varphi_{i+1} = \varphi_i + \Delta\varphi^\sigma(E_{i+1}), \tag{4}$$

where $E_i = H(q(t_i))$, $\varphi_i = \varphi(q(t_i))$. The energy and phase changes $\Delta\varphi^\sigma(E_{i+1})$ and $\Delta H^\sigma(\varphi_i)$ are

$$\Delta\varphi^\sigma(E_{i+1}) \approx \Omega T_\sigma(E_{i+1}) \quad \text{and} \quad \Delta H^\sigma(\varphi_i) \approx \int_{t_i}^{T_\sigma(E_i)+t_i} [H_0, H_1]\,\mathrm{d}t = \int_{t_i}^{T_\sigma(E_i)+t_i} (f_1 g_2 - f_2 g_1)\,\mathrm{d}t, \tag{5}$$

where $[\cdot, \cdot]$ denotes the Poisson bracket. With equation (5), equation (4) is termed the accurate whisker map. The energy and phase changes for equation (1) over one period T_σ of the σ-orbit are explained in Figure 4. In equation (4), the energy increment for the system in equation (1) over one period is obtained approximately, but the phase change is expressed through the exact expressions of natural frequencies instead of their approximations near the separatrix in references [2, 6, 10]. With equation (5), equation (4) will be used for deriving the accurate standard map later on. The second equation in equation (5) can reduce to the energy increment along the separatrix as $T_\sigma \to \infty$, which was used in the traditional standard map in references [2, 10]. As $T_\sigma \to \infty$, it implies that the σ-orbits $(\sigma = \alpha, \beta, \gamma)$ approach to the separatrix, and the energy increment along the separatrix is computed by

$$\Delta H^h(\varphi_i) \approx \lim_{T_\sigma \to \infty} \int_{t_i}^{T_\sigma(E_i)+t_i} [H_0, H_1]\,\mathrm{d}t = \lim_{T_\sigma \to \infty} \int_{t_i}^{T_\sigma(E_i)+t_i} (f_1 g_2 - f_2 g_1)\,\mathrm{d}t, \tag{6}$$

given in references [9, 10]. Equation (6) is used in the traditional standard map only for the computation of the energy change along the separatrix in references [2, 10]. The energy increment in equation (6) is the same as the splitting distance defined through the Melnikov

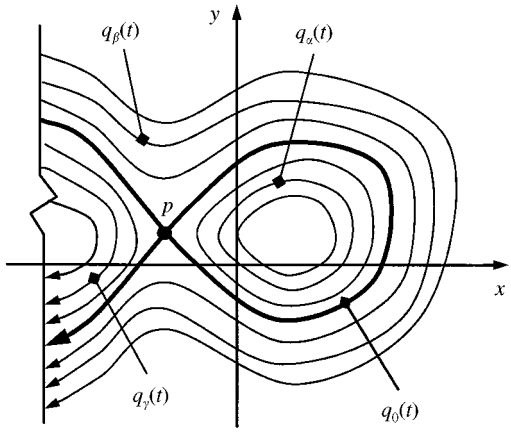

Figure 2. Three families of periodic orbits in the vicinity of the separatrix $q_0(t)$. The bold solid curve represents the separatrix $q_0(t)$. The solid curve gives α-orbit, β-orbit and γ-orbit $(q_\alpha(t), q_\beta(t)$ and $q_\gamma(t))$.

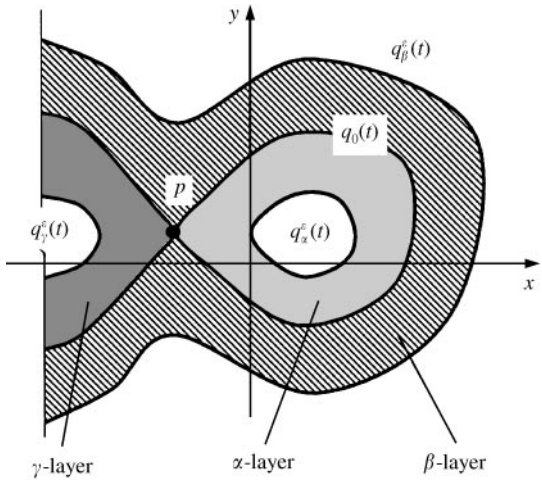

Figure 3. A stochastic layer of equation (1) formed by the Poincare mapping points of $q(t)$ in the ε-neighborhood. The separatrix separates the stochastic layer into three sub-layers, α-, β- and γ-layers.

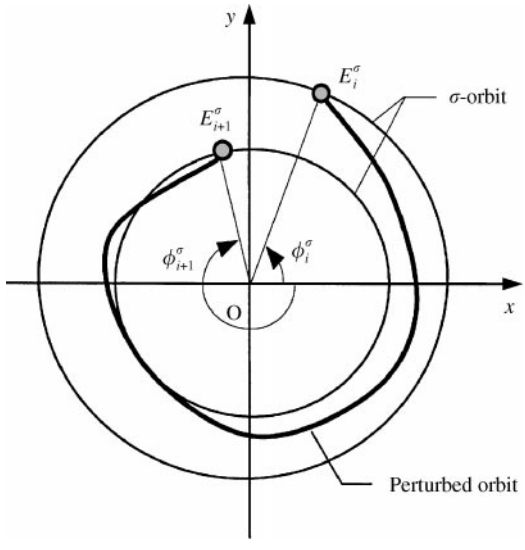

Figure 4. The energy and phase changes of a perturbed orbit over one period T_{σ} based on E^{σ}_{i}.

function [29]. Equation (6) is a special case of equation (5) as the unperturbed orbits approach the separatrix. Therefore, equation (5) used in this paper is applicable for computations of all the energy increments pertaining to the unperturbed periodic orbits in the neighborhood of the separatrix, and through equation (5), similar results can be derived as in reference [29]. In 1990, Luo and Han [4] presented an improved, traditional standard map (or called the approximate standard map). Equation (6) was employed for energy change computation. Although the improved, traditional standard map approach gives a possible prediction of the onset of resonance in the stochastic layer compared to the traditional standard map, it does not agree well with the numerical results when excitation becomes strong. Such an improved traditional standard map approach will be given through the sample problem in the next section.

The resonant condition relative to the unperturbed σ-orbit for a non-linear Hamiltonian system with a periodical excitation [2, 30] is

$$m_\sigma \omega_\sigma = n_\sigma \Omega, \;\; m_\sigma, n_\sigma \in \aleph \text{ are irreducible,} \tag{7}$$

where $\omega_\sigma = 2\pi/T_\sigma$ is a frequency of the σ-orbit, Ω is the excitation frequency and $\aleph$ is the natural number set. The resonant number sets in the stochastic layer for $\sigma = \{\alpha, \beta, \gamma\}$ are introduced:

$$R_\sigma^\varepsilon = \{(m_\sigma : n_\sigma) | m_\sigma \omega_\sigma = n_\sigma \Omega, m_\sigma, n_\sigma \in \aleph \text{ are irreducible, and } |q_\sigma(t) - q_0(t)| < \varepsilon\}. \tag{8}$$

As in references [2, 10], linearization of equation (4) at the period-1 fixed point of the $(m_\alpha : n_\alpha)$ resonance occurs at $E_{i+1} = E_i = E_\alpha^{m_\alpha/n_\alpha}$ and $\varphi_{i+1} = \varphi_i + 2\pi m_\alpha/n_\alpha = \varphi_\sigma^{(m_\sigma : n_\sigma)} + 2\pi m_\alpha/n_\alpha$, thus, equation (4) becomes

$$\Delta\varphi^\sigma(E_\sigma^{(m_\alpha : n_\sigma)}) \approx \frac{2\pi m_\sigma}{n_\sigma} \quad \text{and} \quad \Delta H^\sigma(\varphi_\sigma^{(m_\alpha : n_\sigma)}) = 0, \tag{9}$$

from which $\varphi_\sigma^{(m_\sigma : n_\sigma)}$ and $E_\sigma^{(m_\sigma : n_\sigma)}$ can easily be determined. Perturbation of energy at $E_\sigma^{(m_\sigma : n_\sigma)}$, $E_i = E_\sigma^{(m_\sigma : n_\sigma)} + \Delta E_i$, in equation (4), and use of equation (9) gives

$$w_{i+1} = w_i + G_\sigma^{(m_\sigma : n_\sigma)} \Delta H^\sigma(\varphi_i) \quad \text{and} \quad \varphi_{i+1} \approx \varphi_i + w_{i+1}, \tag{10}$$

where $w_i = G_\sigma^{(m_\sigma : n_\sigma)} \Delta E_i$ and $G_\sigma^{(m_\sigma : n_\sigma)} = \partial[\Delta\varphi(E_{i+1})]/\partial E_{i+1}|_{E_{i+1} = E_\sigma^{(m_\sigma : n_\sigma)}}$. Equation (10) is a generalized accurate standard map. In the derivation of equation (10), following the conventional linearization procedure in reference [10], the phase change in equation (4) is linearized, based on the exact resonant frequency satisfying equation (8), which is shown later in the sample problem. As in references [3–5], the resonant conditions can be derived from the energy analysis of equation (1), and all the unperturbed *σ-orbits* ($\sigma = \alpha, \beta, \gamma$) relative to resonant conditions in three σ-domains are used. However, for the traditional standard map in references [6, 10], the resonant condition is selected arbitrarily, and only one of three unperturbed *σ-orbits* is used.

The criterion for the $(m_\alpha : n_\alpha)$-resonant overlap creating a resonant-separatrix web in the stochastic layer for equation (1) can be obtained through investigation of the exact transition of the local to global stochasticity of equation (10). For determination of that exact transition, those methods presented in references [2, 7, 31, 32] can be employed. For instance, Greene [31, 32] developed a residual method for finding the exact transition of the local to global stochasticity when the last KAM torus is destroyed. Such a method can be used to obtain critical values for the appearance of global stochasticity relative to the $(m_\alpha : n_\alpha)$-resonance. Other approaches presented in reference [2] can be used such as renormalization techniques including loss of stability at rational iterations of the golden mean.

For a specified $G_\alpha^{m_\alpha/n_\alpha} \Delta H_0^\alpha(\varphi_i) = K \sin\varphi_i$, equation (10) reduces to a traditional standard map (or the Chirikov–Taylor map), i.e.,

$$w_{i+1} = w_i + K \sin\varphi_i \quad \text{and} \quad \varphi_{i+1} \approx \varphi_i + w_{i+1}. \tag{11}$$

For the foregoing, the strength of the stochasticity parameter is $K = K^* \approx 0{\cdot}9716\ldots$ in references [31, 32] for the transition to global stochasticity in equation (11). Therefore, for the special case, the perturbation strength of equation (1) is estimated from

$$G_\sigma^{(m_\sigma : n_\sigma)} \Delta H^\sigma(\varphi_{i_i}) \approx 0{\cdot}9716\ldots. \tag{12}$$

3. DUFFING OSCILLATOR

Consider the twin-well-potential Duffing oscillator as an example of a periodically forced, non-linear, Hamiltonian system to verify the accurate standard-map approach:

$$\ddot{x} - \alpha_1 x + \alpha_2 x^3 = Q_0 \cos(\Omega t), \tag{13}$$

where $\alpha_1 > 0, \alpha_2 > 0$ and Q_0 and Ω are excitation strength and frequency. The Hamiltonian of equation (13) is $H = H_0 + H_1$:

$$H_0 = \tfrac{1}{2}\dot{x}^2 - \tfrac{1}{2}\alpha_1 x^2 + \tfrac{1}{4}\alpha_2 x^4 \quad \text{and} \quad H_1 = -xQ_0 \cos(\Omega t). \tag{14}$$

The saddle point of equation (13) is (0,0) and the energy of separatrix is $E_0 = 0$. The homoclinic-orbit, α- and β-orbit of the unperturbed equation (13) can be determined. The α- and β-orbits are located inside and outside of the separatrix, termed the inner and outer orbits. For the inner orbit ($H_0 = E_\alpha < E_0$), the energy E_α, the response amplitude e_α, the natural frequency ω_α and the resonant condition [13] are

$$E_\alpha = \frac{(k^2-1)\alpha_1^2}{(2-k^2)^2\alpha_2}, \quad e_\alpha = \sqrt{\frac{2\alpha_1}{(2-k^2)\alpha_2}}, \quad \omega_\alpha = \frac{\sqrt{\alpha_2}e_\alpha\pi}{\sqrt{2}K(k)}, \quad \omega_\alpha = m\Omega. \tag{15}$$

For the outer orbit ($H_0 = E_\beta > E_0$), and the energy E_β, the response amplitude e_β, the natural frequency ω_β and the resonant condition [13] are

$$E_\beta = \frac{(1-k^2)k^2\alpha_1^2}{(2k^2-1)^2\alpha_2}, \quad e_\beta = \sqrt{\frac{2k^2\alpha_1}{(2k^2-1)\alpha_2}}, \quad \omega_\beta = \frac{\sqrt{\alpha_2}e_\beta\pi}{2\sqrt{2}kK(k)}, \quad \omega_\beta = (2n-1)\Omega. \tag{16}$$

The energy increments of the perturbed orbit in the inner stochastic layer should be computed through two inner orbits possessing the same energy in the two potential wells. Therefore, the energy increment along the $(m:1)$ resonance of the inner orbit is

$$\Delta H_0^\alpha(\varphi_0) = 2\int_{t_0}^{T_\alpha + t_0} (f_1 g_2 - f_2 g_1)\,\mathrm{d}t \approx 2\sqrt{\frac{2}{\alpha_2}}\,Q_0\pi\Omega\,\mathrm{sech}\left(\frac{m\pi K'(k_\alpha^m)}{K(k_\alpha^m)}\right)\sin\varphi_0, \tag{17}$$

where $\varphi_0 = \Omega t_0$, $K'(k_\alpha^m) = K(k_\alpha'^m)$, $k_\alpha'^m = \sqrt{1-(k_\alpha^m)^2}$, and

$$f_1 = \dot{x}, f_2 = \alpha_1 x - \alpha_2 x^3, \quad g_1 = 0, \quad g_2 \grave{Q}_0 \cos(\Omega t). \tag{18}$$

In a like manner, the energy increment along the $(2n-1:1)$-resonance of the outer orbit is

$$\Delta H_0^\beta(\varphi_0) \approx 2\sqrt{\frac{2}{\alpha_2}}\,Q_0\pi\Omega\,\mathrm{sech}\left(\frac{(2n-1)\pi K'(k_\beta^{2n-1})}{2K(k_\beta^{2n-1})}\right)\sin\varphi_0. \tag{19}$$

The energy increment along the homoclinic orbit is obtained from equations (17) and (19):

$$\Delta H_0^h(\varphi_0) = \lim_{T_\alpha\to\infty} \Delta H_0^\alpha = \lim_{T_\beta\to\infty} \Delta H_0^\beta(\varphi_0)$$

$$\approx 2\sqrt{\frac{2}{\alpha_2}}\,Q_0\pi\Omega\,\mathrm{sech}\left(\frac{\pi\Omega}{2\sqrt{\alpha_1}}\right)\sin\varphi_0. \tag{20}$$

3.1. AN ACCURATE STANDARD-MAP APPROACH

3.1.1. *The inner stochastic layer*

The phase change and the modulus is, from equation (15),

$$\Delta\varphi^{\alpha}(E_{\alpha}) = \frac{2\pi\Omega}{\omega_{\alpha}} = \frac{2\Omega\sqrt{2-k^2}K(k)}{\sqrt{\alpha_1}} \quad \text{and} \quad k = \sqrt{\frac{2\sqrt{\alpha_1^2+4\alpha_2 E_{\alpha}}}{\alpha_1+\sqrt{\alpha_1^2+4\alpha_2 E_{\alpha}}}}. \tag{21}$$

Substitution of equation (21) into equation (9) for the $(m:1)$ resonance produces

$$\varphi_0 = 0, \pi \quad \text{and} \quad \Omega\sqrt{2-(k_{\alpha}^m)^2}K(k_{\alpha}^m) = m\pi\sqrt{\alpha_1}\,. \tag{22}$$

Equations (21) and (22) give $E_{\alpha} = E_{\alpha}^m$. From equations (12), (17) and (19), the excitation strength for the onset of resonant overlap in the inner stochastic layer is

$$Q_0 \approx \frac{0{\cdot}4858}{\pi\Omega G_{\alpha}^m}\sqrt{\frac{\alpha_2}{2}}\cosh\left(\frac{\mathrm{m}\pi K'(k_{\alpha}^m)}{K(k_{\alpha}^m)}\right), \tag{23}$$

where

$$G_{\alpha}^m = -\frac{\Omega\alpha_2}{(k_{\alpha}^m)^4}\left(\frac{2-(k_{\alpha}^m)^2}{\alpha_1}\right)^{5/2}\left[2K(k_{\alpha}^m) - \frac{2-(k_{\alpha}^m)^2}{1-(k_{\alpha}^m)^2}E(k_{\alpha}^m)\right], \tag{24}$$

and $E(k_{\alpha}^m)$ is the second elliptic integral with modulus k_{α}^m.

3.1.2. *The outer stochastic layer*

The phase change and the modulus k are

$$\Delta\varphi^{\beta}(E_{\beta}) = \frac{2\pi\Omega}{\omega_{\beta}} = \frac{4\Omega\sqrt{2k^2-1}K(k)}{\sqrt{\alpha_1}} \quad \text{and} \quad k = \sqrt{\frac{\alpha_1\sqrt{\alpha_1^2+4\alpha_2 E_{\beta}}}{2\sqrt{\alpha_1^2+4\alpha_2 E_{\beta}}}}. \tag{25}$$

Substitution of equation (25) into equation (9) for the $(2n-1:1)$ resonance yields

$$\varphi_0 = 0, \pi \quad \text{and} \quad 2\sqrt{2(k_{\beta}^{2n-1})^2-1}\,K(k_{\beta}^{2n-1}) = (2n-1)\pi\sqrt{\alpha_1}\,. \tag{26}$$

With equation (25), the solution to equation (26) is $E_{\beta} = E_{\beta}^{2n-1}$. Equations (12), (19) and (26) gives the excitation strength for the onset of the $(2n-1:1)$-resonance overlap in the outer stochastic layer:

$$Q_0 \approx \frac{0{\cdot}4858}{\pi\Omega G_{\beta}^{2n-1}}\sqrt{\frac{\alpha_2}{2}}\cosh\left(\frac{(2n-1)\pi K'(k_{\beta}^{2n-1})}{2K(k_{\beta}^{2n-1})}\right), \tag{27}$$

where

$$G_{\beta}^{2n-1} = -\frac{2\Omega\alpha_2}{(k_{\beta}^{2n-1})^2}\left(\frac{2(k_{\beta}^{2n-1})^2-1}{\alpha_1}\right)^{5/2}\left[K(k_{\beta}^{2n-1}) - \frac{1-2(k_{\beta}^{2n-1})^2}{1-(k_{\beta}^{2n-1})^2}E(k_{\beta}^{2n-1})\right]. \tag{28}$$

The excitation strengths in equations (23) and (27) distinguish themselves. It indicates that the distinction of the *inner* and *outer* stochastic layers is very significant for a good prediction of the resonant characteristics of the stochastic layer.

3.2. AN APPROXIMATE STANDARD MAP METHOD

The approximate standard map method was developed in references [4, 13]. The procedure is also shown herein for a comparison of this approximate method with the accurate approach presented in the previous section.

3.2.1. *The inner stochastic layer*

As $k \to 1$, the first complete elliptic integral is approximated as in references [7, 10],

$$K(k) \approx \frac{1}{2}\log\left(\frac{16}{1-k^2}\right). \tag{29}$$

From the foregoing, the energy E_α in equation (15) and an approximate period T_α become

$$E_\alpha \approx \frac{(k^2-1)\alpha_1^2}{\alpha_2}, \quad T_\alpha = \frac{2\pi}{\omega_\alpha} \approx \frac{1}{\sqrt{\alpha_1}}\log\left(\frac{16\alpha_1^2}{\alpha_2|\,E_\alpha|}\right). \tag{30}$$

The phase change for one period T_α is

$$\Delta\varphi(E_\alpha) = \Omega T_\alpha \approx \frac{\Omega}{\sqrt{\alpha_1}}\log\left(\frac{16\alpha_1^2}{\alpha_2|\,E_\alpha|}\right). \tag{31}$$

Substituting of equations (20) and (31) into equation (4) yields an approximate whisker map:

$$E_{i+1} \approx E_i + 2Q_0\pi\Omega\sqrt{\frac{2}{\alpha_2}}\,\mathrm{sech}\left(\frac{\pi\Omega}{2\sqrt{\alpha_1}}\right)\sin\varphi_i, \quad \varphi_{i+1} \approx \varphi_i + \frac{\Omega}{\sqrt{\alpha_1}}\ln\left(\frac{16\alpha_1^2}{\alpha_2|\,E_{i+1}|}\right). \tag{32}$$

As in references [4, 13], setting $E_{i+1} = E_i = E_\alpha^m$ and $\varphi_{i+1} = \varphi_i + 2m\pi = \varphi_\alpha^m + 2m\pi$ for the $(m:1)$ resonance in equation (32) gives

$$2Q_0\pi\Omega\,\mathrm{sech}\left(\frac{\pi\Omega}{2\sqrt{\alpha_1}}\right)\sin\varphi_\alpha^m = 0, \quad \frac{\Omega}{\sqrt{\alpha_1}}\ln\left(\frac{16\alpha_1^2}{\alpha_2|\,E_\alpha^m|}\right) = 2m\pi. \tag{33}$$

Solutions to equation (33) for E_α^m and φ_α^m are

$$|E_\alpha^m| = \frac{16\alpha_1^2}{\alpha_2}\,\mathrm{e}^{-(2m\pi\sqrt{\alpha_1}/\Omega)}, \quad \varphi_\alpha^m = 0, \pi. \tag{34}$$

Perturbation of the energy at E_α^m in equation (32) ($E_i = E_\alpha^m + \Delta E_i$) and $w_i = -\Omega\Delta E_i/(\sqrt{\alpha_1}|E_\alpha^m|)$ gives a standard map in equation (11). The strength of stochasticity becomes

$$K = \frac{2Q_0\pi\Omega^2}{\sqrt{\alpha_1}|E_\alpha^m|}\sqrt{\frac{2}{\alpha_2}}\,\mathrm{sech}\left(\frac{\pi\Omega}{2\sqrt{\alpha_1}}\right). \tag{35}$$

From equation (12), the excitation strength for the onset of the $(m:1)$ resonant overlap in the inner stochastic layer is

$$Q_0 \approx \frac{7{\cdot}7728}{\pi}\left(\frac{\alpha_1}{\Omega}\right)^2\sqrt{\frac{\alpha_1}{2\alpha_2}}\,\mathrm{e}^{-[2m\pi\sqrt{\alpha_1}/\Omega]}\cosh\left(\frac{\pi\Omega}{2\sqrt{\alpha_1}}\right). \tag{36}$$

For $\alpha_1 = 2, \alpha_1 = 1$ at $\Omega \ll 1$, equation (36) gives one-half of the result given in references [24, 33]. This is because only one of the two potential wells in equation (13) was considered in reference [24].

3.2.2. *The outer stochastic layer*

The energy E_β in equation (16) and an approximate period T_β, as $k \to 1$, are

$$E_\beta \approx \frac{\alpha_1^2}{\alpha_2}(1-k^2), \quad T_\beta \approx \frac{2}{\sqrt{\alpha_2}} \log\left(\frac{16\alpha_1^2}{\alpha_2 E_\beta}\right). \tag{37}$$

The phase change over one period T_β is

$$\Delta\varphi(E_\beta) = \Omega T_\beta \approx \frac{2\Omega}{\sqrt{\alpha_1}} \log\left(\frac{16\alpha_1^2}{\alpha_2 E_\beta}\right). \tag{38}$$

Substituting equations (20) and (38) into equation (4) yields,

$$E_{i+1} \approx E_i + 2Q_0\pi\Omega\sqrt{\frac{2}{\alpha_2}}\,\mathrm{sech}\left(\frac{\pi\Omega}{2\sqrt{\alpha_1}}\right)\sin\varphi_i, \quad \varphi_{i+1} \approx \varphi_i + \frac{2\Omega}{\sqrt{\alpha_1}}\log\left(\frac{16\alpha_1^2}{\alpha_2 E_{i+1}}\right). \tag{39}$$

Similarly, for $E_{i+1} = E_i = E_\beta^{2n-1}$ and $\varphi_{i+1} = \varphi_i + 2(2n-1)\pi = \varphi_\alpha^{2n-1} + 2(2n-1)\pi$, equation (39) becomes

$$2Q_0\pi\Omega\sqrt{\frac{2}{\alpha_2}}\,\mathrm{sech}\left(\frac{\pi\Omega}{2\sqrt{\alpha_1}}\right)\sin\varphi_\beta^{2n-1} = 0, \quad \frac{2\Omega}{\sqrt{\alpha_1}}\log\left(\frac{16\alpha_1^2}{\alpha_2 E_\beta^{2n-1}}\right) = 2(2n-1)\pi. \tag{40}$$

Solving the foregoing gives E_β^{2n-1} and φ_β^{2n-1}, i.e.,

$$E_\beta^{2n-1} = \frac{16\alpha_1^2}{\alpha_2}\,\mathrm{e}^{-(2n-1)\pi\sqrt{\alpha_1}/\Omega}, \quad \varphi_\beta^{2n-1} = 0, \pi. \tag{41}$$

In a similar fashion, linearization of equation (39) at E_β^{2n-1} with $w_i = -2\Omega\Delta E_i/(\sqrt{\alpha_1}E_\beta^{2n-1})$ yields equation (11). Thus, the stochasticity parameter K is given by

$$K = \frac{4Q_0\pi\Omega^2}{\sqrt{\alpha_1}E_\beta^{2n-1}}\sqrt{\frac{2}{\alpha_2}}\,\mathrm{sech}\left(\frac{\pi\Omega}{2\sqrt{\alpha_1}}\right). \tag{42}$$

The excitation strength for the onset of the $(2n-1:1)$ resonant overlap in the outer stochastic layer is

$$Q_0 = \frac{3{\cdot}8864}{\pi}\left(\frac{\alpha_1}{\Omega}\right)^2\sqrt{\frac{\alpha_1}{2\alpha_2}}\,\mathrm{e}^{-[(2n-1)\pi\sqrt{\alpha_1}/\Omega]}\cosh\left(\frac{\pi\Omega}{2\sqrt{\alpha_1}}\right) \tag{43}$$

The excitation strengths in equations (36) and (43) also distinguish themselves.

3.3. ILLUSTRATIONS

The energy spectrum approach developed in reference [5] is used for numerical predictions, and the accurate, analytical predictions of excitation strength Q_0 are given

through equations (23) and (27), and the approximate predictions through equations (36) and (43). In Figure 5, the solid line gives the accurate prediction of excitation strength Q_0 at $\alpha_1 = \alpha_2 = 1{\cdot}0$ for $\max_\alpha|E_\alpha - E_0| = 0{\cdot}055$ and $\max_\beta|E_\beta - E_0| = 0{\cdot}076$ relative to the modulus $k = 0{\cdot}9684$ close to $k = 1$ for the separatrix. The dashed line represents the approximate prediction of Q_0. The hollow-circle line gives the numerical results generated by the energy spectrum method. The two predictions of Q_0 through two standard-map approaches are very close, but both of them are different from the numerical results because of the phase linearization and energy increment approximation in the neighborhood of the resonant separatrix. If the constraints $\max_\alpha|E_\alpha - E_0| = 0{\cdot}055$ and $\max_\beta|E_\beta - E_0| = 0{\cdot}076$ at $\alpha_1 = \alpha_2 = 1{\cdot}0$ do not apply to the analytical predictions, the excitation strength versus the excitation frequency is illustrated in Figure. 6.

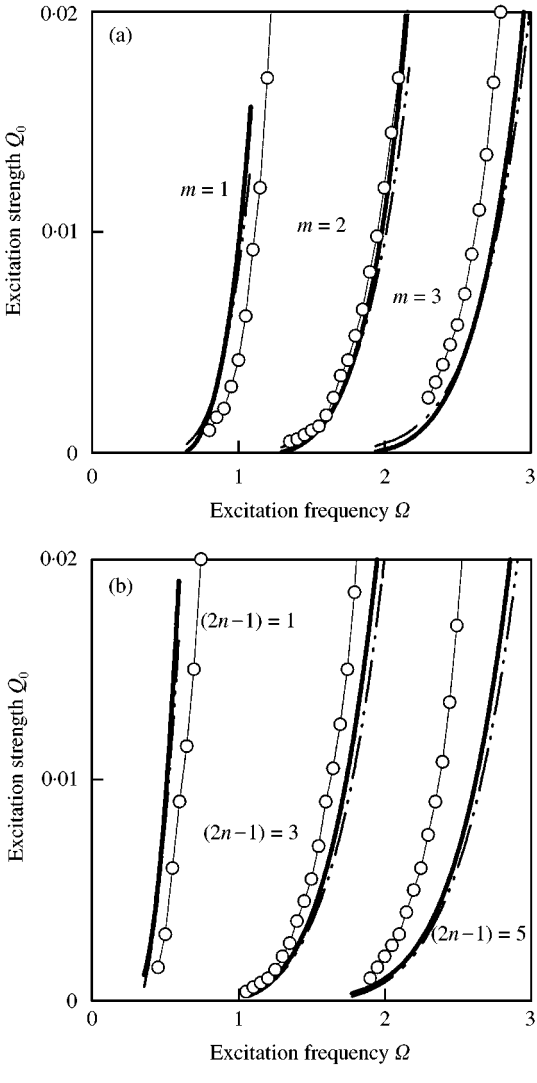

Figure 5. Excitation strengths for (a) the inner layer with $\max|E_\alpha - E_0| = 0{\cdot}055$ and (b) the outer layer with $\max|E_\beta - E_0| = 0{\cdot}076$ in the Duffing oscillator ($\alpha_1 = \alpha_2 = 1{\cdot}0$); ——, accurate; —··—··, approximate; —○—○—, numerical.

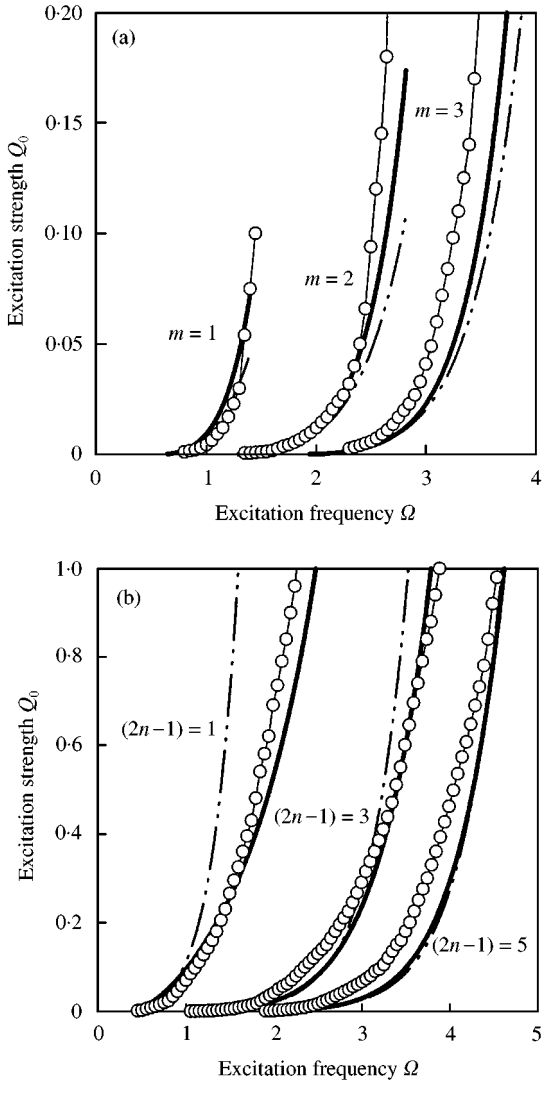

Figure 6. Excitation strength for (a) the inner and (b) the outer layers in the Duffing oscillator ($\alpha_1 = \alpha_2 = 1{\cdot}0$): ——, accurate; —··—, approximate; —○—○—, numerical.

Compared with the numerical results, the accurate standard-map approach gives a much better prediction than the approximate standard-map approach (or the improved *traditional* standard map). When the excitation become strong, the *approximate* standard map gives predictions poorer than the *accurate standard map.* With increasing the order number of resonance, the analytical prediction given by that approximate map becomes poor too. Note that the *traditional* standard map hinged on the *traditional* whisker map cannot provide any correct predictions. We cannot compute any results to make a comparison with the proposed accurate approach because the *traditional* standard map [7, 10] used two equations instead of six equations of the energy and phase changes of the σ-orbits ($\sigma = \alpha, \beta, \gamma$) in the improved traditional standard maps.

3.4. SIMULATIONS

The numerical simulations of stochastic layer are generated by using a second order symplectic scheme [34, 35] with time step $\Delta t = 10^{-5}$–$10^{-7}T$ (where $T = 2\pi/\Omega$ is the perturbation period) and a precision of 10^{-6}. The stochastic layers are illustrated through the Poincare mapping sections defined like

$$\Sigma = \left\{(x(t_N), \dot{x}(t_N))|\text{satisfying equation (13), and } t_N = \frac{2N\pi}{\Omega} + t_0, N = 0, 1, 2, \ldots\right\}, \quad (44)$$

where $x(t_N) = x_N$, $\dot{x}(t_N) = \dot{x}_N$, and $x(t_0) = x_0$, $\dot{x}_0(t_0) = \dot{x}_0$ at $t = t_0$ are initial condition. The Poincare map is $P : \Sigma \to \Sigma$. From equation (44), the stochastic layers are generated through the differential equation (equation (13)) instead of the discrete map for the initial conditions

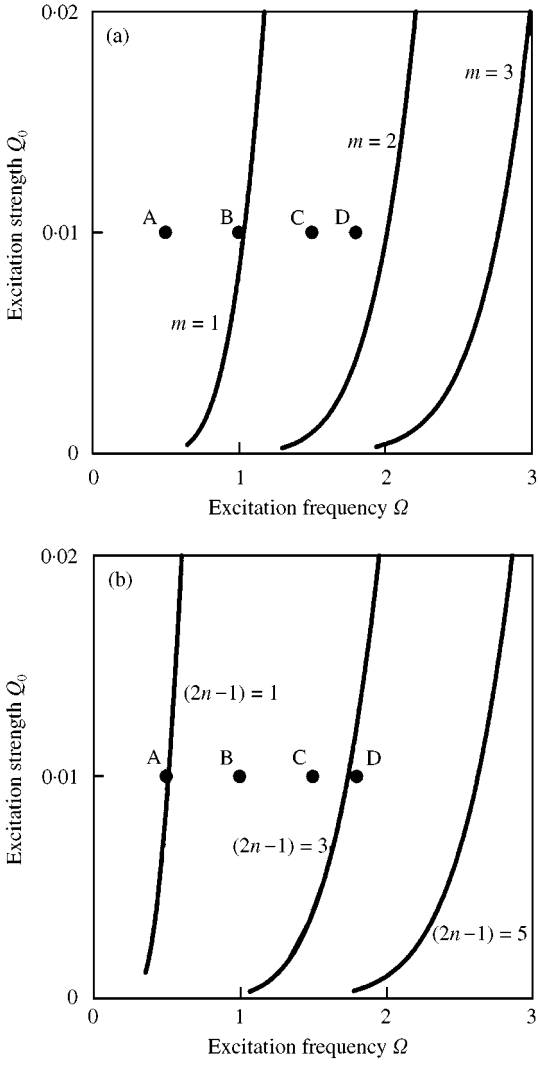

Figure 7. Selection of (Q_0, Ω) at points A–D for numerical simulations of stochastic layers. ($\alpha_1 = \alpha_2 = 1$). The two graphs are for (a) the inner layer and (b) the outer layer.

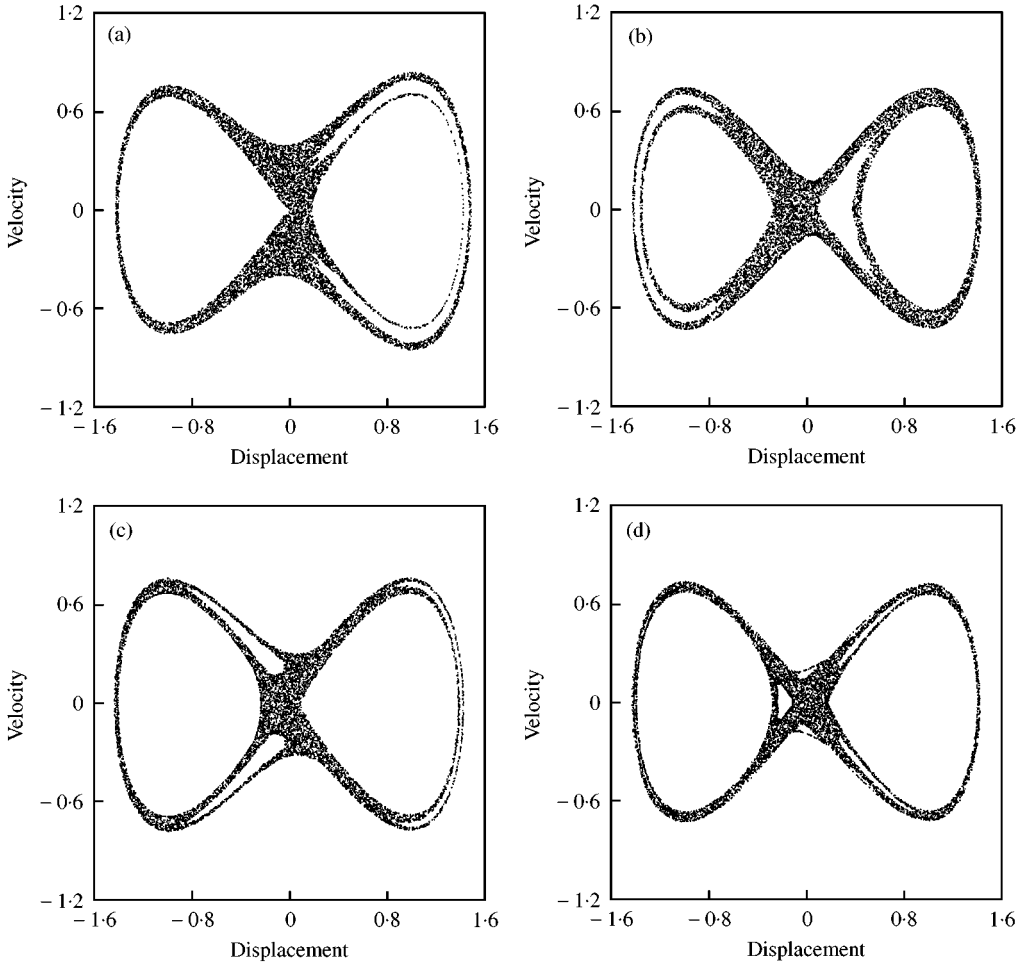

Figure 8. Poincare mapping sections of the stochastic layers in the Duffing oscillator ($\alpha_1 = \alpha_2 = 1{\cdot}0$) at $Q_0 = 0{\cdot}01$: (a) point A, $\Omega = 0{\cdot}5$. (b) point B, $\Omega = 1{\cdot}0$, (c) point C, $\Omega = 1{\cdot}5$, (d) point D, $\Omega = 1{\cdot}8$.

(0,0). When the excitation strength is constant ($Q_0 = 0{\cdot}01$), the excitation frequencies for numerical simulations are selected and marked by the points A–D in Figure 6. The top and bottom graphs of Figure 7 give (Ω, Q_0) for the inner and outer layers. At point A ($\Omega = 0{\cdot}5$), the first order ($m = 1$) resonant overlap is very weak and the resonant-separatrix web is very difficult to be observed in the inner layer. On the other hand, in the bottom graph of Figure 7, it is shown that the first order ($2n - 1 = 1$) resonant overlap is very strong, and it implies that the resonant-separatrix web will appear in the outer layer. This evidence is clearly shown in Figure 8(a). When the excitation frequency increases to $\Omega = 1{\cdot}0$ (point B), a very strong, first order ($m = 1$) resonant overlap appears in the inner layer, but the third order ($2n - 1 = 3$) resonant overlap becomes very weak in the outer layer. Therefore, the resonant-separatrix web of the first order ($m = 1$) exists in the inner layer, as illustrated in Figure 8(b). At point $C(\Omega = 1{\cdot}5)$, the excitation frequency further increases to $\Omega = 1{\cdot}5$, and similarly, the second order ($m = 2$) resonant overlap in the inner layer is weaker than the third order ($2n - 1 = 3$) resonant overlap in the outer layer. Therefore, the third order ($2n - 1 = 3$) resonant-separatrix web in the outer layer will be clearer than the second order

web ($m = 2$) in the inner layer. Such a stochastic layer characterized by the resonance-separatrix web is plotted in Figure 8(c). Finally, at point $D(\Omega = 1{\cdot}8)$, the second order ($m = 2$) resonant overlap in the inner layer is much stronger than the fifth order ($2n - 1 = 5$) resonant overlap in the outer layer, and the second order ($m = 2$) resonant-separatrix web in the inner layer is shown in Figure 8(d).

4. CONCLUSIONS

The onset of a new resonant-overlap in stochastic layers of non-linear Hamiltonian systems with periodical excitations is predicted analytically through the accurate and approximate standard-map approaches. The accurate approach gives a very good prediction compared to the numerical predictions for the lower order resonant overlap. When the excitation is very weak, both of the two standard-map methods are in good agreement. The accurate approach is still applicable to one-degree-of-freedom non-linear Hamiltonian systems with strong, periodical excitations, but the further improvement should be completed for a more accurate, analytical prediction of the onset of a new resonant overlap in stochastic layers. The methodology presented in this paper is applicable for general non-linear Hamiltonian systems.

REFERENCES

1. M. HENON and C. HEILES 1964 *Astronomical Journal* **69**, 73–79. The applicability of the third integral of motion: some numerical experiments.
2. A. J. LICHTENBERG and M. A. LIEBERMAN 1992 *Regular and Chaotic Dynamics*. New York: Springer-Verlag.
3. R. P. S. HAN and A. C. J. LUO 1998 *American Society of Mechanical Engineers, Journal Applied Mechanics* **65**, 727–736. Resonant layers in nonlinear dynamics.
4. A. C. J. LUO and R. P. S. HAN 1999 *Journal of Sound and Vibration* **227**, 523–544. Analytical predictions of chaos in a nonlinear rod.
5. A. C. J. LUO, K. GU and R. S. P. HAN 1999 *Nonlinear Dynamics* **19**, 37–48. The resonant-separatrix webs in stochastic layers of the twin-well Duffing oscillator.
6. G. M. ZASLAVSKY and N. N. FILONENKO 1968 *Soviet Physics JETP* **27**, 851–857. Stochastic instability of trapped particles and conditions of application of the quasi-linear approximation.
7. N. N. FILONENKO, R.. Z. SAGDEEV and G. M. ZASLAVSKY 1967 *Nuclear Fusion* **7**, 253–266. Destruction of magnetic surfaces by magnetic field irregularities: Part II.
8. H. POINCARE 1999 *Les Methods Nouvelles de la Mecanique Celests*. Paris: Gauthier-Zvillars.
9. V. I. ARNOLD 1964 *Soviet Mathematics-Doklady* **5**, 581–585. Instability of dynamical systems with several degrees of freedom.
10. B. V. CHIRIKOV 1979 *Physics Report* **52**, 263–379. A universal instability of many-dimensional oscillator systems.
11. V. K. MELNIKOV 1963 *Transactions Moscow Mathematics Society* **12**, 1–57. On the stability of the center for time periodic perturbations.
12. V. V. VECHESLAVOV 1996 *Soviet Physics JETP* **82**, 1190–1195. Motion in the vicinity of the separatrix of a nonlinear resonance in the presence of high-frequency excitations.
13. A. C. J. LUO 1995 *Ph.D. Dissertation, University of Manitoba, Manitoba, Canada*. Analytical modeling of bifurcations, chaos, and multifractals in nonlinear dynamics.
14. A. C. J. LUO and R. P. S. HAN 2000 *Chaos, Solitons, and Fractals* **11**, 2349–2359. The dynamics of stochastic and resonant layers in a periodically driven pendulum (in press).
15. G. M. ZASLAVSKY and S. S. ABDULLAEV 1995 *Physics Review* **15**, 3901–3910. Scaling properties and anomalous transport of particles inside the stochastic layer.
16. S. S. ABDULLAEV and G. M. ZASLAVSKY 1995 *Physics Plasmas* **2**, 4533–4541. Self-similarity of stochastic magnetic field lines near the X-point.
17. S. S. ABDULLAEV and G. M. ZASLAVSKY 1996 *Physics Plasmas* **3**, 516–528. Application of the separatrix map to study perturbed magnetic field lines near the separatrix.

18. T. AHN, G. KIM and S. KIM 1996 *Physica D* **89**, 315–328. Analysis of the separatrix map in Hamiltonian systems.
19. A. IOMIN and S. FISHMAN 1996 *Physical Review* **54**, R1-R5. Semiclassical quantization of a separatrix map.
20. V. ROM-KEDAR 1990 *Physica D* **43**, 229–268. Transport rates of a class of two-dimensional maps and flow.
21. V. ROM-KEDAR 1994 *Nonlinearity* **7**, 441–473. Homoclinic tangles–classification and applications.
22. V. ROM-KEDAR 1995 *Chaos* **5**, 385–401. Secondary homoclinic bifurcation theorems.
23. D. V. TRESCHEV 1998 *Physica D* **116**, 21–43. Width of stochastic layers in near-integrable two-dimensional symplectic maps.
24. L. E. REICHL and W. M. ZHENG 1984 *Physical Review* **29A**, 2186–2193. Field-induced barrier penetration in the quadratic potential.
25. L. E. REICHL and W. M. ZHENG 1984 *Physical Review* **30A**, 1068–1077. Perturbed double-well system: the pendulum approximation and low-frequency effect.
26. D. F. ESCANDE and F. DOVEIL 1981 *Physical Letter* **83A**, 307–310. Renormalization method for the onset of stochasticity in a Hamiltonian system.
27. D. F. ESCANDE 1985 *Physics Report* **121**, 165–261. Stochasticity in classic Hamiltonian systems: universal aspects.
28. W. A. LIN and L. E. REICHL 1986 *Physica D* **19**, 145–152. External field induced chaos in an infinite square well potential.
29. R. ABRAHAM and J. E. MARSDEN 1978 *Foundations of Mechanics*, London: The Benjamin/Cummings Publishing Company.
30. P. HOLMES, J. MARSDEN and J. SCHEURLE 1988 *Contemporary Mathematics* **81**, 213–244. Exponentially small splittings of separatrices with applications to KAM theory and degenerate bifurcation.
31. J. M. GREENE 1968 *Journal of Mathematics* **9**, 760–768. Two-dimensional measure-preserving mappings.
32. J. M. GREENE 1979 *Journal of Mathematical Physics* **20**, 1183–1201. A method for computing the stochastic transition.
33. L. E. REICHL 1992 *The Transition to Chaos in Conservative Classic System*: *Quantum Manifestations*. New York: Springer-Verlag.
34. K. FENG and M. Z. QIN 1991 *Computational Physics Communications* **65**, 173–187. Hamiltonian algorithms for Hamiltonian systems and a comparative numerical study.
35. R. MCLACHLAN and P. ATELA 1992 *Nonlinearity* **5**, 541–562. The accuracy of symplectic integrators.